J Appl Biotechnol Rep. 2024 December;11(4):1449-1460

Journal of
Applied Biotechnology Reports

doi 10.30491/jabr.2024.487251.1805

Original Article

A Green and Low-Cost Nanocomposite Using Corn Cob Fiber and $ZnFe_2O_4$ for Pesticide Adsorption from Water

Nazila Gholipour [1], Moein Valian [1], Mohammad Hadi Baghersad [2*]

[1] Faculty of Pharmacy, Baqiyatallah University of Medical Sciences, Tehran, Iran
[2] Applied Biotechnology Research Center, Baqiyatallah University of Medical Sciences, Tehran, Iran

Corresponding Author: Mohammad Hadi Baghersad, PhD, Assistant Professor, Applied Biotechnology Research Center, Baqiyatallah University of Medical Sciences, Tehran, Iran. Tel: +989120059822, E-mail: hadibaghersad@bmsu.ac.ir

Received November 5, 2024; **Accepted** December 17, 2024; **Online Published** December 30, 2024

Abstract

Introduction: This study synthesized a nanocomposite using corn cob fiber and $ZnFe_2O_4$, characterized by electron microscopy, X-ray diffraction, infrared spectroscopy, and surface porosity analysis. The research focused on evaluating the adsorption capacity and kinetics of this nanocomposite for removing malathion and bendiocarb, representing organophosphate and carbamate pesticides, respectively.

Materials and Methods: The nanocomposite was prepared and characterized using various techniques. Adsorption experiments assessed the removal efficiency of the pesticides under different conditions, including contact time, initial pollutant concentration, pH, and nanocomposite dosage. Kinetic studies utilized pseudo-first-order (PFO) and pseudo-second-order (PSO) models.

Results: Rapid adsorption occurred within the first 20 minutes, with removal efficiencies of 45.4% for malathion and 40.5% for bendiocarb. Final efficiencies reached 49.3% for malathion and 47.7% for bendiocarb at 85 minutes. Optimal contact times were around 30 minutes for malathion and 40 minutes for bendiocarb. The PSO model provided a better fit, with higher equilibrium adsorption capacities (116.3 mg/g for malathion and 129.9 mg/g for bendiocarb). pH had a positive but minor effect on removal efficiency, and a dosage-dependent increase was observed, with a saturation point beyond 10 mg of nanocomposite.

Conclusions: The corn cob fiber and $ZnFe_2O_4$ nanocomposite effectively removed malathion and bendiocarb from aqueous solutions. Key factors influencing adsorption included contact time, pH, and nanocomposite dosage, highlighting the nanocomposite's potential for pesticide removal applications.

Keywords: Pesticides, Organophosphates, Carbamates, Nanocomposites, Adsorption

Citation: Gholipour N, Valian M, Ranjbari N, Baghersad MH. A Green and Low-Cost Nanocomposite Using Corn Cob Fiber and ZnFe2O4 for Pesticide Adsorption from Water. J Appl Biotechnol Rep. 2024;11(4):1449-1460. doi:10.30491/jabr.2024.487251.1805

Introduction

Nowadays, various pesticides are used to control pests and insects in agricultural fields, increasing the economic productivity of this industry. Organophosphates and carbamates are two important groups of these pesticides that, in addition to their benefits for agriculture, can cause complications in different populations, including humans and other mammals, by contaminating drinking water sources.[1] Both groups of pesticides inhibit the enzyme cholinesterase, leading to cholinergic symptoms such as miosis, rhinorrhea, dyspnea, convulsions, and even death, depending on the contamination level.[2,3] These pesticides also damage the central nervous system and cause peripheral nerve dysfunction.[4] Poisoning from organophosphates is generally more severe and lasts longer than that from carbamates.

Organophosphorus pesticides are widely used as herbicides, fungicides, and nematicides.[5] They inhibit acetylcholinesterase by forming a covalent bond with the hydroxyl group of the amino acid serine in the enzyme's active site, causing a central cholinergic crisis with peripheral symptoms such as tearing, salivation, neuromuscular, and respiratory problems, potentially leading to coma and death.[6] Malathion, a commonly used organophosphorus pesticide, improves agricultural productivity but poses serious risks to humans. Symptoms of malathion poisoning include headache, respiratory problems, and dizziness. Continuous exposure during pregnancy can lead to fetal poisoning. Acute toxicity of malathion can inhibit cholinesterase, causing severe cholinergic symptoms, respiratory paralysis, and death. Malathion can persist in the environment for months and is associated with chronic effects, neurological damage, genetic disorders, carcinogenicity, endocrine disruption, and fertility issues.[7] Exposure to malathion significantly increases DNA damage in humans and other species.[8] Carbamate pesticides, derivatives of carbamic acid, have a similar pest control mechanism to organophosphorus pesticides but pose less risk to mammals. However, their persistence in water and agricultural fields adversely affects plants and beneficial microorganisms, necessitating effective methods to remove

Copyright © 2024 The Author(s). This is an open-access article distributed under the terms of the Creative Commons Attribution License (http://creativecommons.org/licenses/by/4.0), which permits unrestricted use, distribution, and reproduction in any medium, provided the original work is properly cited.

these pesticide residues from the environment.[9,10] Bendiocarb is a carbamate insecticide widely used for pest control in agriculture and public health. Bendiocarb functions as an acetylcholinesterase inhibitor, disrupting the nervous system of insects. It is effective against a broad spectrum of pests, including those affecting maize and sugar beet crops, as well as domestic pests. Due to its relative stability and potential for environmental accumulation, bendiocarb poses significant risks to human health and ecosystems. Residues of this insecticide in soil and water can enter the food chain, causing harm to living organisms. For example, bendiocarb can leach into groundwater, affecting drinking water quality. Additionally, its accumulation in soil can reduce biodiversity and harm soil-dwelling organisms.[11]

Given the significant risks associated with pesticide contamination, it is crucial to develop effective methods for removing these substances from the environment. Various adsorbents have been explored for this purpose, each with unique properties and advantages. Among these, biochar, activated carbon, graphene, bentonite, zeolite, chitosan, and nanoparticles are widely used for removing organic pollutants from aquatic environments.[12-14] Commercial activated carbon is the most common sorbent due to its high sorption capacity. However, its expensive preparation, involving costly feedstocks, high temperatures, and subsequent activation treatments, has led to the development of alternative low-cost sorbents.[15,16] Biochar, derived from the thermochemical treatment of lignocellulosic wastes, offers high surface area, wide sources of raw materials (e.g., rice husk, wheat bran, sawdust, peanut shell, walnut shell, oak bark, pine cone), low cost, and high environmental stability.[17-19] The diameter of many pesticides is smaller than the size of biochar pores, facilitating their absorption. Despite their effectiveness, biochar requires centrifugation or filtration for removal from aqueous solutions, complicating industrial-scale applications.[19-21]

Recent studies have incorporated inorganic or organic compounds into carbonaceous matrices to create hybrid materials with bifunctional properties.[22-24] For example, magnetite nanoparticles impart magnetic properties to carbonaceous materials, aiding in post-sorption recovery using a simple magnet.[25] Iron oxides (Fe_2O_3 and Fe_3O_4) have gained attention for their magnetic properties and effectiveness in removing pollutants, including heavy metals, radioactive materials, and dyes. Adding materials like ZnO and SiO_2 to iron oxide enhances pollutant removal efficiency.[26,27] Yi et al. prepared magnetic biochar from rice straw to sorb crystal violet.[28] The material showed efficient removal percentages of 97%. The kinetics fitting (by pseudo-first and pseudo-second-order models) and the characterization results (by XPS, XRD, Raman analysis, and FTIR) suggested that the main sorption mechanisms are π-π, H-bonding, and electrostatic interactions. Furthermore, Huang et al. synthesized magnetic biochars (from rice straw (M-RHB) and sewage sludge (M-SSB)) that were compared with the non-magnetic biochars (RHB and SSB) for the sorption of Cd^{2+}.[29] After magnetization of the biochars, the sorption capacities decreased from 58.65 (RSB) and 7.22 mg L^{-1} (SSB) to 42.48 (M-RSB) and 4.64 mg L^{-1} (M-SSB). Another research study used empty fruit bunch, a residue from the palm oil industry of Malaysia, to synthesize magnetic biochar by the microwave heating technique.[30] The obtained material had a high surface area of 890 m^2 g^{-1} and was demonstrated to be highly efficient for methylene blue removal of about 99.9% from an aqueous solution.

Recent advancements in the development of nanocomposites for environmental applications underscore the potential of using agricultural waste materials and metal oxides. For instance, a study by Luo et al. demonstrated the enhanced mechanical properties of composites derived from various parts of corn stalks, including cobs, due to their high cellulose and lignin content.[31] Additionally, research on Zn/ZnO modified cellulosic nanocomposites has shown their efficiency and eco-friendliness in wide-scale applications.[32] The integration of $ZnFe_2O_4$ with carbon-based materials has also been explored for its photocatalytic and pollutant removal capabilities.[33] Spinel ferrites with the general molecular formula MFe_2O_4 (M=Zn, Co, Mn) have higher resistance in critical acidic and alkaline conditions and have been used as photocatalysts for the removal of nitroaromatic compounds in water.[34] They also have photocatalytic properties on some microorganisms that can act as disinfectants. Among the ferrites, $ZnFe_2O_4$ composite with carbon has been prepared and has shown suitable pollutant removal efficiency.[35,36]

These studies provide a strong foundation for the development of green and low-cost nanocomposites, such as the one proposed in this work, which aims to utilize corn cob fiber and $ZnFe_2O_4$ for effective pesticide adsorption from water. So, continuing our previous works.[37-42] we prepared nanocomposites using biochar from corn cob fiber and $ZnFe_2O_4$ with various weight ratios. We evaluated their adsorption capacity for malathion and bendiocarb from water solutions after characterizing them. This approach aims to leverage the high surface area and environmental stability of biochar, combined with the magnetic properties of $ZnFe_2O_4$, to develop an efficient and sustainable method for pesticide removal from contaminated water.

Materials and Methods

Preparation of Corn Cob Biochar

The method of Ding et al. was used to prepare biochar from corn cob fiber.[43] One liter of 68% sulfuric acid was added to 100 g of corn cob fiber and stirred for 10 minutes. This mixture was slowly added to 507 ml of distilled water under stirring and the resulting slurry was filtered. The filtrate was

transferred to a beaker and 347 ml of 98% sulfuric acid was added dropwise under stirring. The beaker was heated at 95 °C for 6 hours with occasional stirring. The mixture was filtered again using a paper filter and the solid residue was collected. The residue was dried in an incubator at 60 °C for 24 hours to obtain biochar from corn cob fiber (6.28 g).

Preparation of $ZnFe_2O_4$

$FeCl_3 \cdot 6H_2O$ (4 mmol) and $ZnCl_2$ (2 mmol) were dissolved in ethylene glycol (70 ml) and ammonium acetate (30 mmol) was added as a protective agent. The mixture was sonicated for 30 minutes and stirred at 600 rpm at room temperature. The mixture was transferred to a 100 ml Teflon-lined stainless-steel autoclave and heated at 210 °C for 48 hours. The system was cooled to room temperature and the black precipitate was collected by magnetic field decantation. The precipitate was washed with ethanol and distilled water several times and dried in a vacuum system at 60 °C for 12 hours.[44] Then the resulting mixture was passed through filter paper, and the solid on the filter was washed alternately six times with ethanol and then with distilled water to remove any possible contaminants. Finally, after drying the solid, 0.22 g of $ZnFe_2O_4$ was obtained.

Preparation of Magnetic Biochar

In this research, three nanocomposites with different weight ratios of corn cob biochar and $ZnFe_2O_4$ were prepared. To prepare the magnetic nanocomposites, the same method as described in section 2.2 was used, with the addition of 0.11 g, 0.22 g, and 0.44 g of biochar prepared in section 2.1 to the mixture before sonication for nanocomposites 1 to 3, respectively. The mixture was then stirred for 10 minutes.

Characterization of Magnetic Biochar

Scanning electron microscopy (SEM, TESCAN S9000, Czech Republic) coupled with energy-dispersive X-ray spectroscopy (EDS, Oxford XMAX, UK) was used to observe the surface morphology of the nanocomposites. A surface analyzer (JW-SEL200, China) was used to analyze the specific surface area and pore size distribution of the nanocomposites. The surface functional groups of the nanocomposites were determined by Fourier transform infrared spectroscopy (FT-IR, Thermo Nicolet 6700, USA). X-ray diffraction (Bruker D8 advance, Germany) was performed to analyze the phase structure of the nanocomposites. Magnetic properties of the nanocomposites were determined by vibrating-sample magnetometry (VSM, LBKFB, Iran). A UV–visible spectrophotometer (Shimadzu, Japan) was used to measure the concentration of malathion and bendiocarb in aqueous solutions.

Effects of $ZnFe_2O_4$ Content on Pesticides Adsorption by Magnetic Biochar

Biochar and magnetic biochar (5 mg) prepared with different corn cob biochar/$ZnFe_2O_4$ weight ratios (2:1, 1:1 and 1:2) were added into a 10-ml serum bottle containing malathion or bendiocarb (initial concentration = the highest concentration of poison that resulted in a clear solution, 68.4 mg/L and 75 mg/L, respectively) and placed into a shaker at a speed of 200 rpm for 120 min (room temperature). The nanocomposite was isolated from the solution by utilizing a magnet, and the concentration of residual poisons was measured by the UV–visible spectrophotometer at 221.1 nm for malathion and 214.4 nm for bendiocarb.

Adsorption Experiments

10 ml of pesticide solution with a known initial concentration was stirred with the optimum amount of magnetic biochar on a shaker operating at 25 °C. Then samples were allowed to settle for 15 minutes under a magnetic field. The concentration of the residual pesticides was measured using a UV–VIS spectrophotometer at the appropriate wavelength corresponding to the maximum absorption of pesticides (221.10 nm for malathion and 214.40 nm for bendiocarb). The percent removal of pesticides from the solution was calculated using the following equation:

$$\text{Removal } (\%) = \frac{C_0 - C_i}{C_0} \times 100$$

Where C0 is the initial concentration of pesticide and Ci is the final concentration of pesticide.

Results and Discussion

Characterizations of the Nanocomposites

The nanocomposites were prepared by mixing zinc ferrite and biochar in different weight ratios, as described in section 2.3. The weight ratio of biochar to zinc ferrite was 1:2 for nanocomposite 1, 1:1 for nanocomposite 2, and 2:1 for nanocomposite 3.

FT-IR Spectroscopy

Figure 1 displays the FT-IR spectra of $ZnFe_2O_4$ and the nanocomposites 1-3. The spectra exhibit absorption bands in the range of 460-740 cm^{-1} for all samples, which correspond to the Zn-O and Fe-O bonds in $ZnFe_2O_4$. The spectra of the nanocomposites 1-3 also show absorption bands of C-O bonds around 1100 cm^{-1} and C-C bond around 1600 cm^{-1}, indicating the presence of biochar in the nanocomposites. The C-H stretching peaks (2900-3000 cm^{-1}) increase in intensity with increasing biochar content, reflecting the higher carbon content in the nanocomposites. The O-H stretching peaks (3200-3600 cm^{-1}) shift slightly to lower wavenumbers with increasing biochar content, suggesting that some hydrogen bonding may have occurred between the hydroxyl groups of biochar and the oxygen atoms of zinc ferrite.

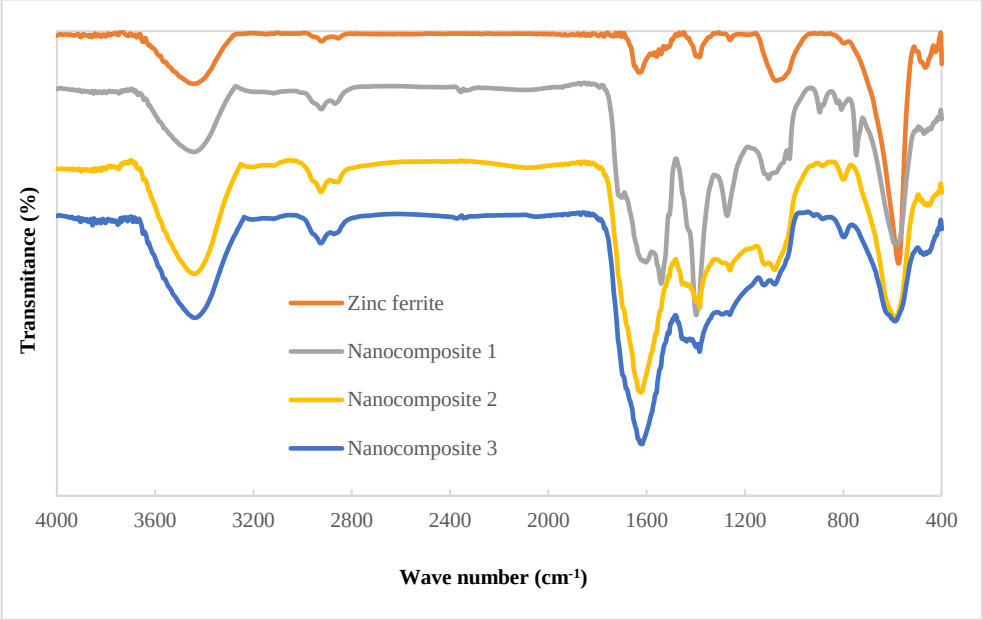

Figure 1. FT-IR Spectra of $ZnFe_2O_4$ and the Synthesized Nanocomposites 1-3.

FE-SEM Analysis

The morphology of zinc ferrite and its nanocomposites with biochar was investigated by electron microscopy, as shown in Figure 2. The zinc ferrite nanoparticles exhibited a spherical shape with a uniform size distribution, indicating a successful crystallization process. The image of nanocomposite 1 revealed a good dispersion of zinc ferrite and biochar nanoparticles, without any noticeable agglomeration. However, for nanocomposites 2 and 3, the increased weight ratio of biochar resulted in a more porous and rougher surface morphology, which could affect the properties of the nanocomposites.

VSM

The hysteresis curves obtained from VSM are shown in Figure 3. These curves show that the production of nanocomposites has reduced the magnetic properties of zinc ferrite. The magnetic moment of zinc ferrite was 50 emu/g, while it was 25 emu/g for nanocomposite 1, and 12.5 emu/g for nanocomposites 2 and 3. This reduction may be due to the pinning effect or the locking of the magnetic domains by biochar. The results suggest that the addition of biochar to zinc ferrite decreases the saturation magnetization (Ms) of the nanocomposites, as evidenced by the decrease in Ms values. The effect of biochar on Ms is proportional to the amount of biochar added, as nanocomposite 1 has the lowest biochar content and the highest Ms value among the nanocomposites, while nanocomposite 3 has the highest biochar content and the lowest Ms value among the nanocomposites.

This may be related to the dilution or shielding effect of biochar on the magnetic domains of zinc ferrite. However, this effect seems to reach a limit when the biochar content reaches a certain level. Nanocomposites 2 and 3 have different biochar contents, but they have the same Ms value. This means that adding more biochar to nanocomposite 2 does not reduce its Ms any further. This may be related to some other factors that counteract or balance out the dilution or shielding effect of biochar on Ms. For example, it is possible that adding more biochar changes the structure or morphology of zinc ferrite particles in a way that enhances their magnetic alignment or interaction. It is also possible that adding more biochar introduces some impurities or defects in zinc ferrite particles that increase their magnetic anisotropy or coercivity. The nanocomposites had very low coercivity at room temperature, which showed that they were superparamagnetic and did not retain any magnetization after the removal of an external magnetic field. The nanocomposites 2 and 3 also had a saturation magnetization of about 12.5 emu/g, which meant that they could be easily and quickly separated by a magnetic field without any residual magnetism.

BET Analysis

The surface area and porosity of the samples were investigated by BET analysis, a technique for measuring gas adsorption on solid surfaces. The results of the BET analysis are summarized in Table 1. The results indicate that the specific surface area and total pore volume increased with the weight ratio of biochar, except for nanocomposite 1, which had a lower pore volume than zinc ferrite. This could be due to the filling effect or the occupation of some pores by biochar particles. The average pore diameter also changed with the addition of biochar, showing a more heterogeneous pore size distribution.

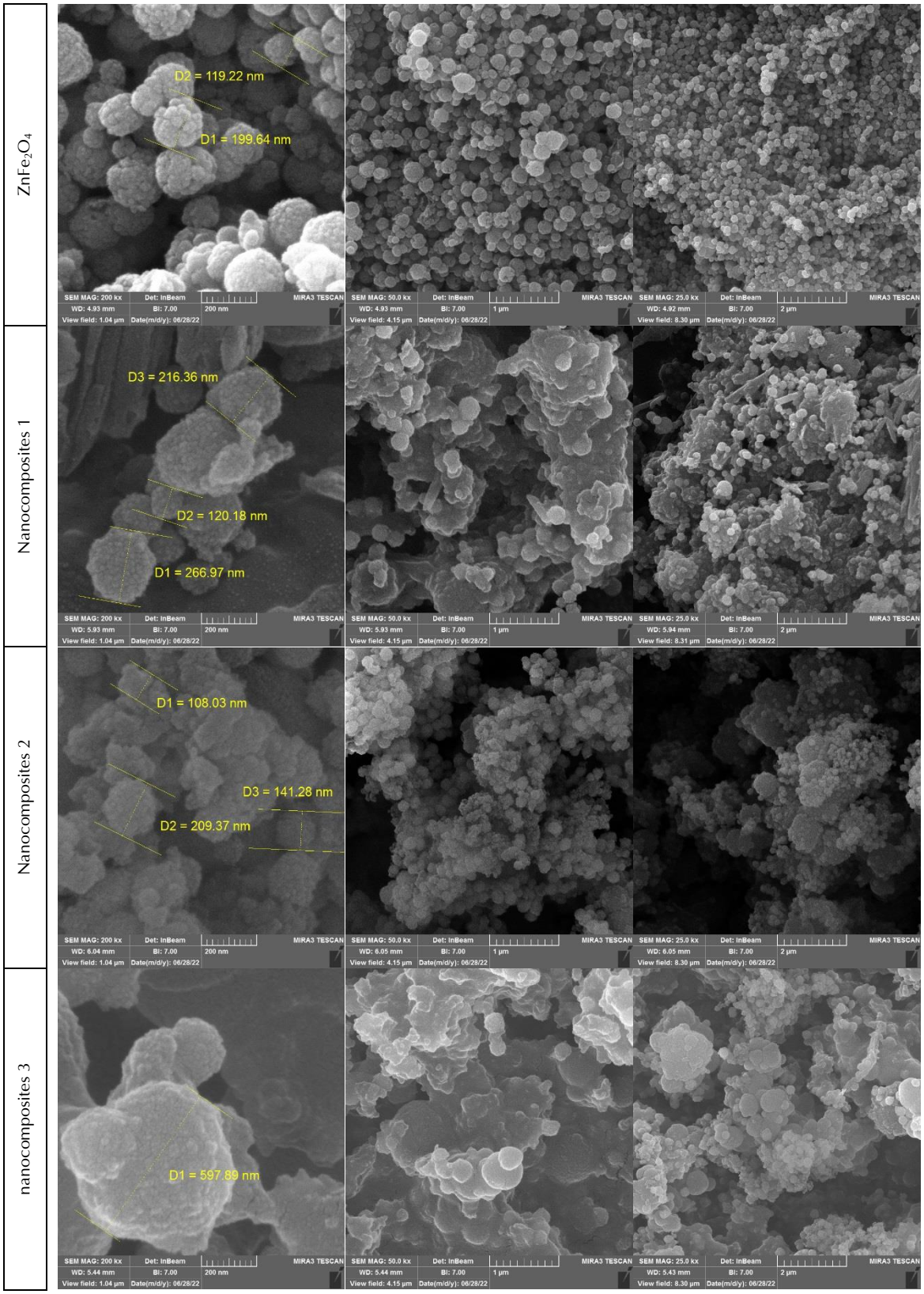

Figure 2. SEM Images of $ZnFe_2O_4$ and the Synthesized Nanocomposites 1-3.

The results suggest that adding biochar to zinc ferrite increases the porosity of the nanocomposites, as seen in the increase in specific surface area and total pore volume. The effect of biochar on the average pore diameter depends on the amount added, with nanocomposite 1 having smaller pores than zinc ferrite, while nanocomposites 2 and 3 have larger pores. This difference may be related to the aggregation or dispersion of biochar particles in the nanocomposites.

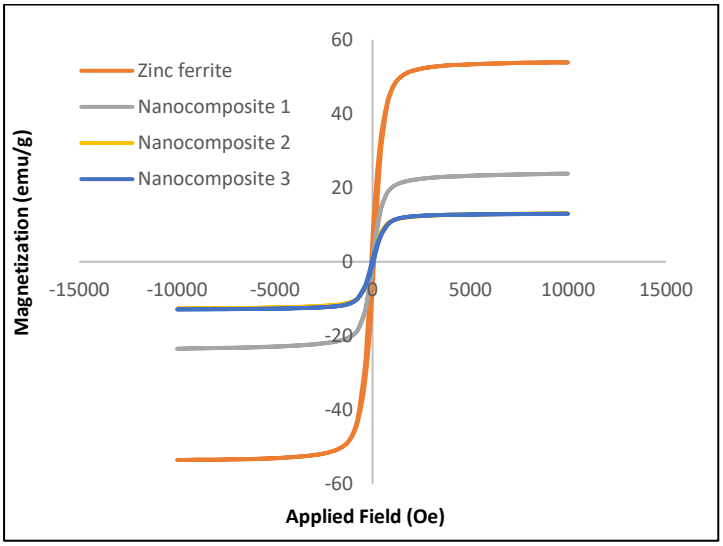

Figure 3. The Hysteresis Curves Obtained from VSM for $ZnFe_2O_4$ and Nanocomposites 1-3.

Table 1. Results of Surface Porosity Analysis for Zinc Ferrite and the Synthesized Nanocomposites 1-3

Sample	$ZnFe_2O_4$	Nanocomposites 1	Nanocomposites 2	Nanocomposites 3
Specific surface area [total area per unit mass] ($m^2\ g^{-1}$)	16.181	19.532	23.291	94.975
Total pore volume per unit mass ($cm^3\ g^{-1}$)	0.064066	0.049917	0.1379	0.2815
Average pore diameter (nm)	15.838	10.223	23.69	11.855

Therefore, it can be expected that nanocomposite 3, with the highest specific surface area and total pore volume among the four samples, would have the highest adsorption capacity for organic pollutants.

XRD Analysis

X-ray diffraction (XRD) is a powerful technique for characterizing the structural and chemical properties of materials. It can provide information about the phase composition, lattice parameters, crystallite size, strain, and preferred orientation of the crystalline phases in a sample. The XRD patterns of the samples are shown in Figure 4.

The biochar addition affects the structural properties of zinc ferrite, causing lattice contraction, crystallite size reduction, strain increase, and phase separation. The biochar phase is mainly composed of amorphous carbon with some graphitic domains, which may have intercalated into the zinc ferrite lattice or formed a thin layer on the surface of the zinc ferrite particles. The biochar may have acted as a nucleating agent and a dispersing agent, promoting the formation of smaller and more uniform zinc ferrite particles with higher surface energy and defect density.

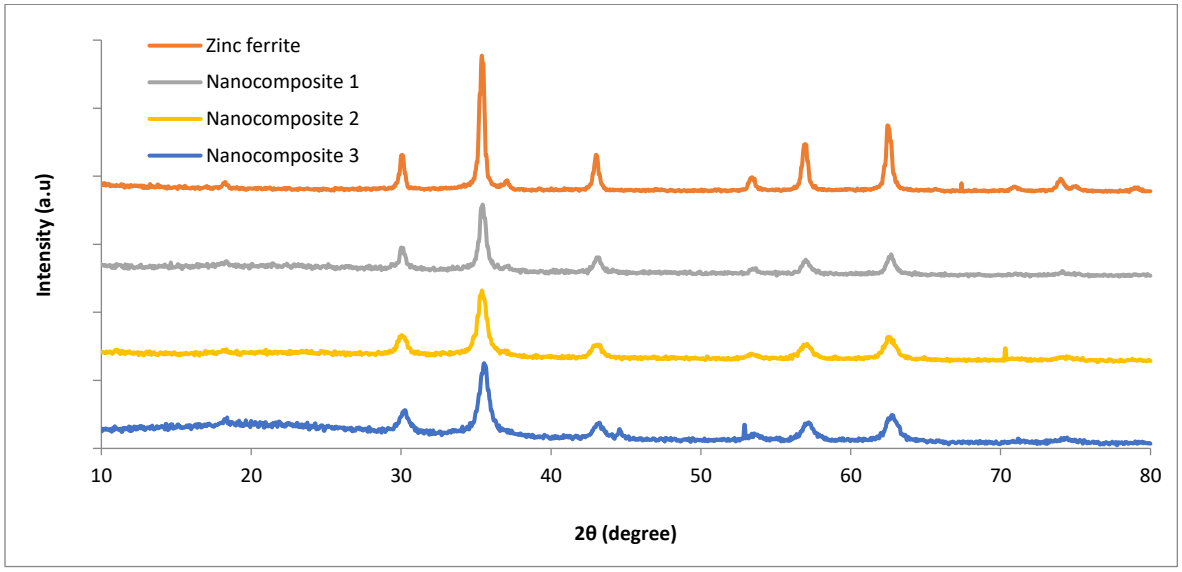

Figure 4. The XRD Pattern of $ZnFe_2O_4$ and the Nanocomposites 1-3.

Selection of the most Suitable Nanocomposite

The removal efficiencies of malathion and bendiocarb pesticides by three nanocomposites (1, 2, and 3) were compared under the same experimental conditions. The nanocomposites were prepared by mixing biochar with different amounts of $ZnFe_2O_4$ nanoparticles, as described in section 3.1. The initial concentrations of the pesticide solutions were 68.4 mg/L for malathion and 75 mg/L for bendiocarb, and the pH was adjusted to 7. Five milligrams of each nanocomposite were added to 10 ml of the pesticide solutions and stirred at room temperature for 40 minutes. The residual concentrations of the pesticides were measured by the UV–visible spectrophotometer at 221.1 nm for malathion and 214.4 nm for bendiocarb, as explained in section 2.5. The investigation of the removal efficiency of both pesticides showed that there was no significant difference between the three synthesized nanocomposites. However, when the specific surface area of the nanocomposites was measured by the Brunauer–Emmett–Teller (BET) method, as described in section 3.1, it was found that nanocomposite 3 had the highest value (94.98 m^2/g), followed by nanocomposite 2 (23.29 m^2/g) and nanocomposite 1 (19.53 m^2/g). This suggests that nanocomposite 3 has more available sites for adsorption than the other two nanocomposites.

Another advantage of nanocomposite 3 is that it has the highest proportion of biochar, which is a low-cost and renewable material, compared to nanocomposite 2 and nanocomposite 1. This makes nanocomposite 3 more economical and environmentally friendly than the other two nanocomposites. Therefore, nanocomposite 3 was selected as the most suitable nanocomposite for further studies.

Removal Efficiency and Adsorption Studies

Effects of Contact Time on Removal Efficiency and Adsorption Kinetic

The removal percentage of malathion and bendiocarb pesticides by the nanocomposite 3 was evaluated over a period of 85 minutes. The initial concentrations of malathion and bendiocarb in their respective 10 ml solutions were 68.4 mg/L and 75 mg/L, with 3 mg of the nanocomposite used for the removal process. The initial concentrations were selected based on the maximum concentrations of malathion and bendiocarb that fall within the linear range of the UV absorbance-concentration curve.

As shown in Figure 5a, the removal efficiency increased rapidly within the first 20 minutes, reaching 45.4% for malathion and 40.5% for bendiocarb. This rapid initial adsorption can be attributed to the availability of abundant active sites on the nanocomposite surface. After 20 minutes, the removal rates began to plateau, with the final removal percentages at 85 minutes being 49.3% for malathion and 47.7% for bendiocarb. The data indicates that nanocomposite 3 was slightly more effective in removing malathion compared to bendiocarb, likely due to differences in their chemical structures and properties. Overall, nanocomposite 3 demonstrated significant potential for pesticide removal, with rapid initial adsorption followed by saturation of adsorption sites over time.

The optimal contact time for the removal of malathion appears to be around 30 minutes, as the removal efficiency stabilizes at approximately 48.5%. For bendiocarb, the optimal contact time is slightly longer, around 40 minutes, where the removal efficiency reaches about 46.3%. Beyond these times, the increase in removal efficiency is minimal, suggesting that the adsorption sites on the nanocomposite become saturated.

To determine the kinetic model that best describes the removal process, two models were tested, including pseudo-first order (PFO) and pseudo-second order (PSO). The linearized forms of these models are given by equations (1) and (2), respectively:

1) $\ln(q_e - q_t) = \ln(q_e) - k_1 t$

2) $t/q_t = 1/k_2 q_e^2 + t/q_e$

Where q_e and q_t are the amounts of pesticide adsorbed at equilibrium and at time t (mg/g), respectively; k_1 and k_2 are the model parameters. The model parameters were estimated by linear regression using GraphPad Prism 8.0.2 software. The correlation coefficients (R^2) were used to evaluate the goodness of fit. The results are summarized in Table 2 and the related curves are shown in Figure 5b.

The adsorption kinetics of malathion and bendiocarb were analyzed using both pseudo-first-order (PFO) and pseudo-second-order (PSO) models. As shown in Table 2, the PFO model yielded rate constants (k_1) of 0.0776 min^{-1} for malathion and 0.0536 min^{-1} for bendiocarb, with correlation coefficients R^2 of 0.7863 and 0.6526, respectively. The equilibrium adsorption capacities (q_e) were 47.1 mg/g for malathion and 37.4 mg/g for bendiocarb. In contrast, the PSO model provided a better fit for the experimental data, with higher R^2 values of 0.9992 for malathion and 0.9990 for bendiocarb. The rate constants (k_2) were 0.0031 g/mg min for malathion and 0.0012 g/mg min for bendiocarb, and the equilibrium adsorption capacities (q_e) were significantly higher at 116.3 mg/g for malathion and 129.9 mg/g for bendiocarb. According to Figure 5b, the time-dependent adsorption data further supports the superiority of the PSO model. For malathion, the PSO model closely predicted the experimental values, with q_e values of 74.52 mg/g at 5 minutes, 90.83 mg/g at 10 minutes, and 112.57 mg/g at 85 minutes. Similarly, for bendiocarb, the PSO model predictions were 56.95 mg/g at 5 minutes, 79.18 mg/g at 10 minutes, and 120.77 mg/g at 85 minutes. The PFO model, however, showed significant deviations from the experimental data, particularly at higher contact times.

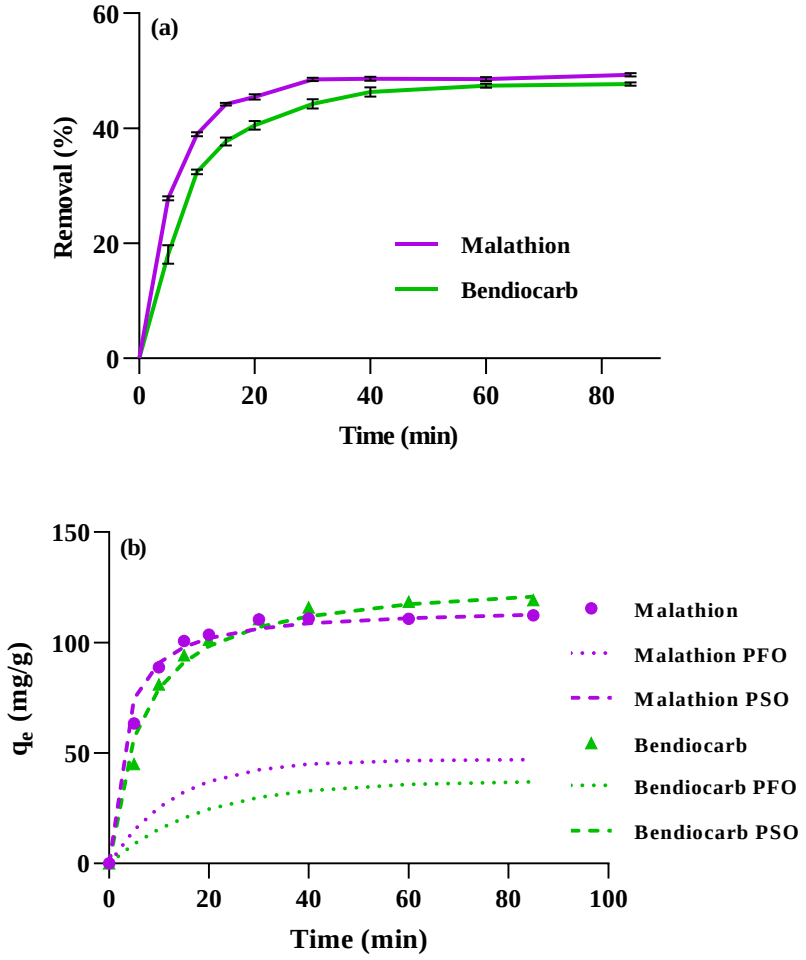

Figure 5. a) Effect of contact time of nanocomposite 3 on the removal capacity of Malathion and bendiocarb (pH = 7, nanocomposite dosage = 3 mg/L, temperature of 298 K, pollutant volume 10 ml); b) Adsorption kinetic (PFO and PSO).

Table 2. Parameters of PFO and PSO Models for the Adsorption of Malathion and Bendiocarb on Nanocomposite 3

Kinetic model	Parameter	Malathion	Bendiocarb
Pseudo-first order	k_1 (min^{-1})	0.0776	0.0536
	R^2	0.7863	0.6526
	q_e (mg/g)	47.1	37.4
Pseudo-second order	k_2 (g/mg min)	0.0031	0.0012
	R^2	0.9992	0.9990
	q_e (mg/g)	116.3	129.9

Effects of pH

To investigate the effect of pH on the removal efficiency of malathion and bendiocarb from aqueous solutions, experiments were conducted using nanocomposite 3. Malathion and bendiocarb solutions with a concentration of 68.4 mg/L and 75.0 mg/L, respectively were prepared at pH levels between 5-9 in volumes of 10 ml, and 3 mg of the nanocomposite was added to each solution. These mixtures were shaken at 160 rpm for 30 minutes for malathion and 40 minutes for bendiocarb. pH levels below 5 and above 9 were avoided due to the increased instability and rapid degradation of both malathion and bendiocarb in these extreme conditions, which could interfere with accurate measurement of adsorption efficiency.[45]

The results showed that while the removal efficiency of both pesticides increased with rising pH levels, the increase was not substantial (Figure 6). At pH 5, the removal efficiencies were 46.9% for malathion and 41.3% for bendiocarb. As the pH increased, the removal efficiencies improved slightly, reaching 48.1% for malathion and 42.9% for bendiocarb at pH 6, and further increasing to 55.2% for malathion and 49.8% for bendiocarb at pH 9. These findings suggest that higher pH levels enhance the adsorption capacity of nanocomposite 3, likely due to increased ionization of the pesticides and greater availability of active sites on the nanocomposite surface. However, while the increased removal efficiency at pH 9 is beneficial, its practical application depends on the specific requirements and constraints of the water treatment process.

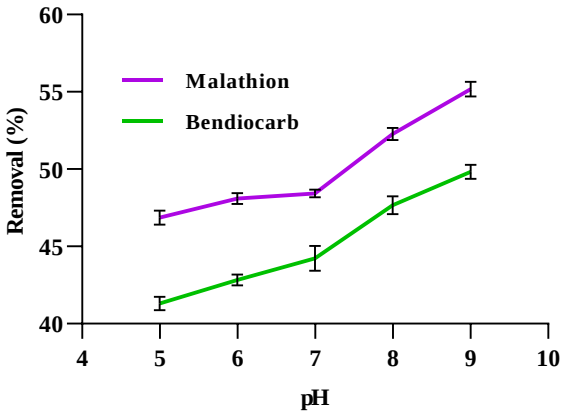

Figure 6. Effect of pH on the Removal Capacity of Malathion and Bendiocarb by Nanocomposite 3.

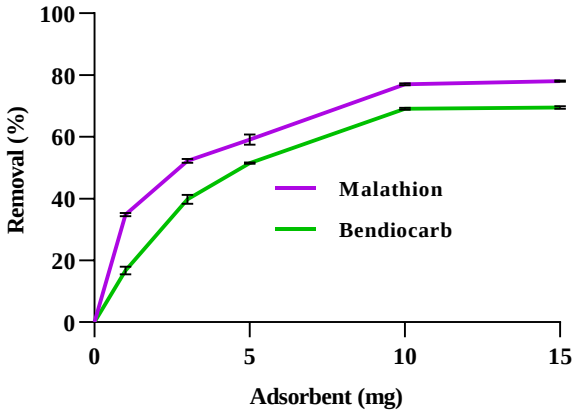

Figure 7. Effect of Adsorbent Dosage on the Removal of Malathion and Bendiocarb by Nanocomposite 3.

Effect of Adsorbent Dosage

The effect of varying adsorbent dosage of nanocomposite 3 (1, 3, 5, 10, and 15 mg) on the removal of malathion and bendiocarb was studied under conditions of pH 7 and a temperature of 298 K. The initial concentrations were set at 136.8 mg/L for malathion and 136 mg/L for bendiocarb in 10 ml solutions (highest possible concentrations that their solutions remained clear). The solutions were then subjected to shaking at 160 rpm for optimal times (30 minutes for malathion and 40 minutes for bendiocarb.

As shown in Figure 7, the results demonstrated a clear dosage-dependent increase in removal efficiency for both pesticides. For malathion, the removal efficiency increased from 34.8% with 1 mg of nanocomposite to 78.0% with 15 mg. Similarly, for bendiocarb, the removal efficiency rose from 16.7% with 1 mg to 69.6% with 15 mg. The optimal removal times were 30 minutes for malathion and 40 minutes for bendiocarb. These findings indicate that higher dosages of nanocomposite 3 significantly enhance the adsorption capacity, likely due to the increased availability of active sites for adsorption. However, the marginal increase in removal efficiency beyond 10 mg suggests a saturation point, where additional adsorbent does not proportionally increase removal efficiency. This highlights the importance of optimizing adsorbent dosage to achieve maximum removal efficiency while considering cost-effectiveness and material usage.

Comparison

The adsorption capacities of different adsorbents for organophosphates (Malathion) and carbamates are summarized in Table 3. The results indicate significant variability in adsorption capacities, highlighting the effectiveness of different materials in removing these contaminants. Due to the limited number of reports on the removal of bendiocarb, we have included data on other carbamates in this table for comparison. This approach allows for a broader understanding of the adsorption capacities of various adsorbents for carbamates. Nanocomposite 3, synthesized in this work using biochar derived from corn cob and zinc ferrite, exhibits notable adsorption capacities for both organophosphates and carbamates, making it a versatile and effective adsorbent. Additionally, it is a magnetic adsorbent, which offers the advantage of easy separation from aqueous solutions using

an external magnetic field. The comparative analysis shows that while Nanocomposite 3 does not achieve the highest adsorption capacities reported, it offers a balanced performance for both organophosphates and carbamates. This dual functionality, combined with the use of sustainable materials like biochar from corn cob and its magnetic properties, makes it a promising candidate for practical applications in environmental remediation. Further optimization and cost analysis will be essential to enhance its applicability and efficiency.

Table 3. Adsorption Capacities of Various Adsorbents for Organophosphates (Malathion) and Carbamates (Including Bendiocarb and Other Carbamates)

Adsorbent	Adsorption Capacity (mg/g)	
	Organophosphates (Malathion)	Carbamates (as footnoted)
TTA-bentonite[46]	16.7	-
Activated carbon[47]	32.1	-
Reduced graphene oxide[48]	68.8	-
Magnetic graphene oxide[49]	43.3	-
Biochar from Jute fibers[50]	71.63	-
Granular activated carbon derived from coconut shell[51]	909.1	-
Granular activated carbon derived from palm shells[51]	555.6	-
Tangerine seed activated carbon[52]	-	7.97 [a]
Graphene quantum dots[53]	-	125 [b]
Chitosan/alginic beads[54]	-	95.71 [b]
Copper-BDC/chitosan/alginic beads[54]	-	225.51 [b]
Zinc Oxide nano particles[55]	-	158.34 [c]
Nanocomposite 3 (This work)	**116.3**	**129.9** [a]

[a] Carbamate: bendiocarb; [b] Carbamate: oxamyl; [c] Carbamate: carbaryl (CBRL)

Conclusion

This study demonstrated that a nanocomposite prepared from corn cob fiber and $ZnFe_2O_4$ is effective in removing malathion and bendiocarb from aqueous solutions. The nanocomposite's properties were characterized using advanced techniques, confirming its suitability for adsorption applications. The removal efficiency increased rapidly within the first 20 minutes due to the abundant active sites on the nanocomposite surface, with optimal contact times identified as 30 minutes for malathion and 40 minutes for bendiocarb. Adsorption kinetics analysis revealed that the pseudo-second-order model provided a better fit for the experimental data, indicating chemisorption as the rate-limiting step. The effect of pH on removal efficiency showed that while higher pH levels enhanced adsorption, the increase was not substantial, suggesting that pH 7 or 8 might be more practical for real-world applications. Additionally, a dosage-dependent increase in removal efficiency was observed, with a saturation point beyond 10 mg of nanocomposite. These findings underscore the importance of optimizing contact time, pH, and adsorbent dosage to maximize removal efficiency while considering economic and environmental factors. Further research should focus on the regeneration and reuse of the nanocomposite to enhance its practical applicability in water treatment processes.

Authors' Contributions

NG: Supervision and project administration, validation, review & editing, visualization; MV: Formal analysis, investigation, provision of study materials, reagents, materials, laboratory samples, instrumentation, computing resources, or other analysis tools; MHB: Co-supervision, conceptualization, methodology, provision of study materials, reagents, materials, laboratory samples, instrumentation, writing original data, visualization and project administration. All authors reviewed and approved the manuscript.

Conflict of Interest Disclosures

The authors declare that they have no conflicts of interest.

References

1. Adisa IO, Pullagurala VL, Peralta-Videa JR, Dimkpa CO, Elmer WH, Gardea-Torresdey JL, et al. Recent advances in nano-enabled fertilizers and pesticides: a critical review of mechanisms of action. Environ Sci Nano. 2019;6(7):2002-30. doi:10.1039/C9EN00265K
2. Tripathi A, Lal S, Kumari P. Carbon Nanomaterials for Adsorption and Desorption of Pesticides. Carbon Nanomaterials and their Composites as Adsorbents. Cham: Springer International Publishing. 2024. pp. 203-227). doi:10.1007/978-3-031-48719-4_12
3. Al-Gethami W, Qamar MA, Shariq M, Alaghaz AN, Farhan A, Areshi AA, et al. Emerging environmentally friendly bio-based nanocomposites for the efficient removal of dyes and micropollutants from wastewater by adsorption: a comprehensive review. RSC Adv. 2024;14 (4):2804-34. doi:10.1039/D3RA06501D
4. Mehta J, Dhaka RK, Dilbaghi N, Lim DK, Hassan AA, Kim KH, et al. Recent advancements in adsorptive removal of organophosphate pesticides from aqueous phase using nanomaterials. J Nanostructure Chem. 2024; 14(1):53-70. doi:10.1007/s40097-022-00516-y
5. Yadav GK, Ahmaruzzaman M. Recent advances in the development of nanocomposites for effective removal of pesticides from aqueous stream. J Nanoparticle Res. 2021;23(9):213. doi:10.1007/s11051-021-05290-6
6. Garba ZN, Abdullahi AK, Haruna A, Gana SA. Risk assessment and the adsorptive removal of some pesticides from synthetic wastewater: a review. Beni-Suef Univ J Basic Appl Sci. 2021;10:19. doi:10.1186/s43088-021-00109-8
7. Huang B, Chen F, Shen Y, Qian K, Wang Y, Sun C, et al. Advances in targeted pesticides with environmentally responsive controlled release by nanotechnology. Nanomaterials. 2018;8(2):102. doi:10.3390/nano8020102

8. Bruckmann FS, Schnorr C, Oviedo LR, Knani S, Silva LF, Silva WL, et al. Adsorption and photocatalytic degradation of pesticides into nanocomposites: a review. Molecules. 2022;27(19):6261. doi:10.3390/molecules27196261
9. Uddin S. Removal of pesticides using carbon-based nanocomposite materials. Environmental Remediation Through Carbon Based Nano Composites. 2021:365-85. doi:10.1007/978-981-15-6699-8_17
10. Sarojini G, Kannan P, Rajamohan N, Rajasimman M, Vo DV. Dyes removal from water using polymeric nanocomposites: a review. Environ Chem Lett. 2023;21(2):1029-58. doi:10.1007/s10311-022-01547-1
11. Mucoz-Martínez S, Ahuatzi-Chacyn D, Santoyo-Tepole F, Ruiz-Ordaz N, Galнndez-Mayer J, Juárez-Ramírez C. Biodegradation of the insecticide bendiocarb by *Bacillus thuringiensis* in a packed biofilm reactor. Appl Biochem Microbiol. 2021;57:S46-53. doi:10.1134/S0003683821100070
12. Rashid R, Shafiq I, Akhter P, Iqbal MJ, Hussain M. A state-of-the-art review on wastewater treatment techniques: the effectiveness of adsorption method. Environ Sci Pollut Res. 2021;28:9050-66. doi:10.1007/s11356-021-12395-x
13. Osman AI, El-Monaem EM, Elgarahy AM, Aniagor CO, Hosny M, Farghali M, et al. Methods to prepare biosorbents and magnetic sorbents for water treatment: a review. Environ Chem Lett. 2023;21(4):2337-98. doi:10.1007/s10311-023-01603-4
14. Nazari MT, Schnorr C, Rigueto CV, Alessandretti I, Melara F, da Silva NF, et al. A review of the main methods for composite adsorbents characterization. Environmental Science and Pollution Research. 2022;29(59):88488-506. doi:10.1007/s11356-022-23883-z
15. Badran AM, Utra U, Yussof NS, Bashir MJ. Advancements in Adsorption Techniques for Sustainable Water Purification: A Focus on Lead Removal. Separations. 2023;10(11):565. doi:10.3390/separations10110565
16. Pillai SB. Adsorption in Water and Used Water Purification, in: Lahnsteiner J (Ed.), Handbook of Water and Used Water Purification, Springer International Publishing, Cham, 2020, pp. 1-22.
17. Muigai HH, Bordoloi U, Hussain R, Ravi K, Moholkar VS, Kalita P. A comparative study on synthesis and characterization of biochars derived from lignocellulosic biomass for their candidacy in agronomy and energy applications. Int J Energy Res. 2021;45(3):4765-81. doi:10.1002/er.6092
18. Wang K, Remyn J, Jiang Z, Ding W. Recent Advances in the Preparation and Application of Biochar Derived from Lignocellulosic Biomass: A Mini Review. Polymers. 2024;16(6):851. doi:10.3390/polym16060851
19. Chaturvedi S, Singh SV, Dhyani VC, Govindaraju K, Vinu R, Mandal S. Characterization, bioenergy value, and thermal stability of biochars derived from diverse agriculture and forestry lignocellulosic wastes. Biomass Conv. Bioref. 2023;13:879-92. doi:10.1007/s13399-020-01239-2
20. Mukherjee A, Patra BR, Podder J, Dalai AK. Synthesis of biochar from lignocellulosic biomass for diverse industrial applications and energy harvesting: effects of pyrolysis conditions on the physicochemical properties of biochar. Front Mater. 2022;9:870184. doi:10.3389/fmats.2022.870184
21. Prochnow FD, Cavali M, Dresch AP, Belli IM, Libardi N, de Castilhos AB. Biochar: From Laboratory to Industry Scale—An Overview of Scientific and Industrial Advances, Opportunities in the Brazilian Context, and Contributions to Sustainable Development. Processes. 2024;12(5):1006. doi:10.3390/pr12051006
22. Polak MP, Kudrawiec R, Jacobs R, Szlufarska I, Morgan D. Modified band alignment method to obtain hybrid functional accuracy from standard DFT: Application to defects in highly mismatched III-V: Bi alloys. Phys Rev Mater. 2021;5(12):124601. doi:10.1103/PhysRevMaterials.5.124601
23. Sephra PJ, Chandrapagasam T, Sachdev A, Esakkimuthu M. Bifunctional properties of Ag/α-Fe2O3/rGO nanocomposite for supercapacitor and electrochemical nitrate sensing using tetradodecyl ammonium nitrate as ion-selective membrane. Environ Sci Pollut Res. 2024;31(40):52886-904. doi:10.1007/s11356-024-34703-x
24. Navrotskaya AG, Aleksandrova DD, Krivoshapkina EF, Sillanpää M, Krivoshapkin PV. Hybrid materials based on carbon nanotubes and nanofibers for environmental applications. Front Chem. 2020;8:546. doi:10.3389/fchem.2020.00546
25. Khan FS, Mubarak NM, Khalid M, Walvekar R, Abdullah EC, Mazari SA, et al. Magnetic nanoadsorbents' potential route for heavy metals removal—a review. Environ Sci Pollut Res. 2020;27:24342-56. doi:10.1007/s11356-020-08711-6
26. Sacko A, Nure JF, Nyoni H, Mamba B, Nkambule T, Msagati TA. The application of tannic acid-coated magnetite nanoparticles for recovery of microplastics from the water system. Water Conserv Sci Eng. 2024;9(2):41. doi:10.1007/s41101-024-00275-7
27. Ojemaye MO, Okoh OO, Okoh AI. Effectiveness of magnetite nanoparticles for the removal of DNA of multidrug-resistant *Escherichia coli* from municipal wastewater. Environ Sci Pollut Res. 2024. doi:10.1007/s11356-024-35098-5
28. Yi Y, Tu G, Ying G, Fang Z, Tsang EP. Magnetic biochar derived from rice straw and stainless steel pickling waste liquor for highly efficient adsorption of crystal violet. Bioresour Technol. 2021;341:125743. doi:10.1016/j.biortech.2021.125743
29. Huang F, Zhang SM, Wu RR, Zhang L, Wang P, Xiao RB. Magnetic biochars have lower adsorption but higher separation effectiveness for Cd2+ from aqueous solution compared to nonmagnetic biochars. Environ Pollut. 2021;275:116485. doi:10.1016/j.envpol.2021.116485
30. Mubarak NM, Kundu A, Sahu JN, Abdullah EC, Jayakumar NS. Synthesis of palm oil empty fruit bunch magnetic pyrolytic char impregnating with FeCl3 by microwave heating technique. Biomass Bioenergy. 2014;61:265-75. doi:10.1016/j.biombioe.2013.12.021
31. Liu L, Chang D, Gao C. A review of multifunctional nanocomposite fibers: design, preparation and applications. Adv Fiber Mater. 2024;6(1):68-105. doi:10.1007/s42765-023-00340-1
32. Wasim M, Shi F, Liu J, Farooq A, Khan SU, Salam A, et al. An overview of Zn/ZnO modified cellulosic nanocomposites and their potential applications. J Polym Res. 2021;28(9):338. doi:10.1007/s10965-021-02689-6
33. Chong TY, Law MC, Chan YS. The potentials of corn waste lignocellulosic fibre as an improved reinforced bioplastic composites. J Polym Environ. 2021;29(2):363-81. doi:10.1007/s10924-020-01888-4
34. Yang W, Chen D, Quan H, Wu S, Luo X, Guo L. Enhanced photocatalytic properties of ZnFe 2 O 4-doped ZnIn 2 S 4 heterostructure under visible light irradiation. RSC Adv. 2016;6(86):83012-9. doi:10.1039/C6RA14847F
35. Wu Y, Wang Y, Di A, Yang X, Chen G. Enhanced photocatalytic performance of hierarchical ZnFe 2 O 4/gC 3 N 4 heterojunction composite microspheres.

Catalysis Letters. 2018;148:2179-89. doi:10.1007/s10562-018-2376-6
36. Li X, Xing H, Yang X, Wang D, Feng J, Zong Y, et al. Construction of ZnFe2O4/g-C3N4 heterojunction as reusable visible-light photocatalyst and the boosted photocatalytic efficiency by photo-self-Fenton effect for organic pollutant degradation. J Mater Sci: Mater Electron. 2023;34(15):1204. doi:10.1007/s10854-023-10640-2
37. Nasiripur P, Zangiabadi M, Baghersad MH. Visible light photocatalytic degradation of methyl parathion as chemical warfare agents simulant via GO-Fe3O4/Bi2MoO6 nanocomposite. J Mol Struct. 2021;1243:130875. doi:10.1016/j.molstruc.2021.130875
38. Jafari S, Dehghani M, Nasirizadeh N, Baghersad MH. Synthesis and characterisation of a selective adsorbent based on the molecularly imprinted polymer for the removal of cloxacillin antibiotic residue from milk. Int J Dairy Technol. 2019;72(4):505-14. doi:10.1111/1471-0307.12620
39. Zangiabadi M, Mehrabi F, Nasiripur P, Baghersad MH. Visible-light-driven photocatalytic degradation of methyl parathion as chemical warfare agent simulant by NiO/Bi2MoO6 heterojunction photocatalyst. J Mol Struct. 2022;1256:132472. doi:10.1016/j.molstruc.2022.132472
40. Baghersad MH, Maleki A, Khodabakhshi MR. Design and development of novel magnetic Lentinan/PVA nanocomposite for removal of diazinon, malathion, and diclofenac contaminants. J Contam Hydrol. 2023;256:104193. doi:10.1016/j.jconhyd.2023.104193
41. Abdollahi R, Goodarzi V, Baghersad MH. Introducing a new co-polymeric adsorbent with fast sorption rate and high sorption capacity for removing the heavy metal ions: A thermodynamic and kinetic study. Scientia Iranica. 2021;28(3):1436-51. doi:10.24200/sci.2020.54302.3691
42. Baghersad M, Dehghani M, Jafari S, Nasirizadeh N. Synthesis and application of a carbon composite containing molecularly imprinted poly (methacrylic acid) for efficient removal of fenpyroximate pesticide. J Environ Sci Health. B. 2022;57(12):917-31. doi:10.1080/03601234.2022.2146959
43. Ding L, Zou B, Liu H, Li Y, Wang Z, Su Y, et al. A new route for conversion of corncob to porous carbon by hydrolysis and activation. J Chem Eng. 2013;225:300-5. doi:10.1016/j.cej.2013.03.090
44. Rahimi R, Kerdari H, Rabbani M, Shafiee M. Synthesis, characterization and adsorbing properties of hollow Zn-Fe2O4 nanospheres on removal of Congo red from aqueous solution. Desalination. 2011;280(1-3):412-8. doi:10.1016/j.desal.2011.04.073
45. Lamb RW, McAlexander H, Woodley CM, Shukla MK. Towards a comprehensive understanding of malathion degradation: comparison of degradation reactions under alkaline and radical conditions. Environ Sci Process Impacts. 2022;24(7):1026-36. doi:10.1039/D2EM00050D
46. Pal OR, Vanjara AK. Removal of malathion and butachlor from aqueous solution by clays and organoclays. Sep Purif Technol. 2001;24(1-2):167-72. doi:10.1016/S1383-5866(00)00226-4
47. Habila MA, ALOthman ZA, Al-Tamrah SA, Ghafar AA, Soylak M. Activated carbon from waste as an efficient adsorbent for malathion for detection and removal purposes. J Ind Eng Chem. 2015;32:336-44. doi:10.1016/j.jiec.2015.09.009
48. Atar N, Eren T, Yola ML, Karimi-Maleh H, Demirdugen B. Magnetic iron oxide and iron oxide@ gold nanoparticle anchored nitrogen and sulfur-functionalized reduced graphene oxide electrocatalyst for methanol oxidation. RSC Adv. 2015;5(33):26402-9. doi:10.1039/C5RA03735B
49. Kalantary RR, Azari A, Esrafili A, Yaghmaeian K, Moradi M, Sharafi K. The survey of Malathion removal using magnetic graphene oxide nanocomposite as a novel adsorbent: thermodynamics, isotherms, and kinetic study. Desalin Water Treat. 2016;57(58):28460-73. doi:10.1080/19443994.2016.1178605
50. Senthilkumaar S, Krishna SK, Kalaamani P, Subburamaan CV, Subramaniam NG. Adsorption of organophosphorous pesticide from aqueous solution using" waste" jute fiber carbon. Mod Appl Sci. 2010;4(6):67.
51. Jusoh A, Hartini WJ, Endut A. Study on the removal of pesticide in agricultural run off by granular activated carbon. Bioresour Technol. 2011;102(9):5312-8. doi:10.1016/j.biortech.2010.12.074
52. Wang Y, Wang SL, Xie T, Cao J. Activated carbon derived from waste tangerine seed for the high-performance adsorption of carbamate pesticides from water and plant. Bioresour Technol. 2020;316:123929. doi:10.1016/j.biortech.2020.123929
53. Agarwal S, Sadeghi N, Tyagi I, Gupta VK, Fakhri A. Adsorption of toxic carbamate pesticide oxamyl from liquid phase by newly synthesized and characterized graphene quantum dots nanomaterials. J Colloid Interface Sci. 2016;478:430-8. doi:10.1016/j.jcis.2016.06.029
54. Abdelhameed RM, Rady A, Elsherbiny AS, Gemeay AH. Effectiveness application of Chitosan/Alginic/Copper–organic framework beads on removal of carbaryl carbamate from wastewater. Environ Nanotechnol Monit Manag. 2023;20:100832. doi:10.1016/j.enmm.2023.100832
55. Sen K, Barik R, Mondal NK. State-of-the-art fabrication of crystalline zinc oxide for carbamate adsorption: Experimental, optimization, and molecular dynamics simulation. Groundw Sustain Dev. 2024;26:101226. doi:10.1016/j.gsd.2024.101226